

Simulation on atmospheric pressure barrier discharge with varying relative position between two wavy dielectric surfaces

Xue-Chen Li(李雪辰), Wen-Jie Wan(万文杰), Xiao-Qian Liu(刘晓倩), Mo Chen(陈墨), Kai-Yue Wu(吴凯玥), Jun-Xia Ran(冉俊霞), Xue-Xia Pang(庞学霞), Xue-Xue Zhang(张雪雪), Jia-Cun Wu(武珈存), Peng-Ying Jia(贾鹏英), and Hui Sun(孙辉)

Citation: Chin. Phys. B, 2025, 34 (**3**): 035202. DOI: 10.1088/1674-1056/ada43d
Journal homepage: http://cpb.iphy.ac.cn; http://iopscience.iop.org/cpb

What follows is a list of articles you may be interested in

Turbulent drag reduction by sector-shaped counter-flow dielectric barrier discharge plasma actuator

Borui Zheng(郑博睿), Shaojie Qi(齐少杰), Minghao Yu(喻明浩), Jianbo Zhang(张剑波), Linwu Wang(王林武), and Dongliang Bian(卞栋梁)
Chin. Phys. B, 2025, 34 (**2**): 025205. DOI: 10.1088/1674-1056/ada1c6

Electron characteristics and dynamics in sub-millimeter pulsed atmospheric dielectric barrier discharge

Junlin Fang(方骏林), Yarong Zhang(张亚容), Chenzi Lu(卢陈梓), Lili Gu(顾莉莉), Shaofeng Xu(徐少锋), Ying Guo(郭颖), and Jianjun Shi(石建军)
Chin. Phys. B, 2024, 33 (**1**): 015201. DOI: 10.1088/1674-1056/ad0118

Flow control performance evaluation of a tri-electrode sliding discharge plasma actuator

Borui Zheng(郑博睿), Yuanpeng Liu(刘园鹏), Minghao Yu(喻明浩), Yuanzhong Jin(金元中),Qian Zhang(张倩), and Quanlong Chen(陈全龙)
Chin. Phys. B, 2023, 32 (**9**): 095203. DOI: 10.1088/1674-1056/acae76

Dynamic stall control over an airfoil by NS-DBD actuation

He-Sen Yang(杨鹤森), Guang-Yin Zhao(赵光银)†, Hua Liang(梁华)‡, and Biao Wei(魏彪)
Chin. Phys. B, 2020, 29 (**10**): 105203. DOI: 10.1088/1674-1056/abb227

Electrical modeling of dielectric barrier discharge considering surface charge on the plasma modified material

Hong-Lu Guan(关弘路), Xiang-Rong Chen(陈向荣), Tie Jiang(江铁), Hao Du(杜浩), Ashish Paramane, Hao Zhou(周浩)
Chin. Phys. B, 2020, 29 (**7**): 075204. DOI: 10.1088/1674-1056/ab8a3f

---

Simulation on atmospheric pressure barrier discharge with varying relative position between two wavy dielectric surfaces

Xue-Chen Li(李雪辰)[1,2], Wen-Jie Wan(万文杰)[1], Xiao-Qian Liu(刘晓倩)[1], Mo Chen(陈墨)[2], Kai-Yue Wu(吴凯玥)[3], Jun-Xia Ran(冉俊霞)[2], Xue-Xia Pang(庞学霞)[4], Xue-Xue Zhang(张雪雪)[4], Jia-Cun Wu(武珈存)[4], Peng-Ying Jia(贾鹏英)[1,2,†], and Hui Sun(孙辉)[5]

[1] *College of Physics Science and Technology, Hebei University, Baoding* 071002, *China*
[2] *Engineering Research Center of Zero-carbon Energy Buildings and Measurement Techniques, Ministry of Education, Baoding* 071002, *China*
[3] *Department of Electrical Engineering, Tsinghua University, Beijing* 100084, *China*
[4] *Hebei Key Laboratory of Photo-Electricity Information and Materials, Hebei University, Baoding* 071002, *China*
[5] *University of Chinese Academy of Sciences, College of Materials and Opto-Electronic Technology, Beijing* 100049, *China*

(Received 15 November 2024; revised manuscript received 24 December 2024; accepted manuscript online 31 December 2024)

As a popular approach to producing atmospheric pressure non-thermal plasma, dielectric barrier discharge (DBD) has been extensively used in various application fields. In this paper, DBD with wavy dielectric layers is numerically simulated in atmospheric pressure helium mixed with trace nitrogen based on a fluid model. With varying relative position (phase difference ($\Delta\varphi$)) of the wavy surfaces, there is a positive discharge and a negative discharge per voltage cycle, each of which consists of a pulse stage and a hump stage. For the pulse stage, maximal current increases with increasing $\Delta\varphi$. Results show that DBD with the wavy surfaces appears as discrete micro-discharges (MDs), which are self-organized to different patterns with varying $\Delta\varphi$. The MDs are vertical and uniformly-spaced with $\Delta\varphi$ =0, which are self-organized in pairs with $\Delta\varphi = \pi/4$. These MD pairs are merged into some bright wide MDs with $\Delta\varphi = \pi/2$. In addition, narrow MDs appear between tilted wide MDs with $\Delta\varphi = 3\pi/4$. With $\Delta\varphi = \pi$, the pattern is composed of wide and narrow MDs, which are vertical and appear alternately. To elucidate the formation mechanism of the patterns with different $\Delta\varphi$, temporal evolutions of electron density and electric field are investigated for the positive discharge. Moreover, surface charge on the wavy dielectric layers has also been compared with different $\Delta\varphi$.

Keywords: dielectric barrier discharge, wavy dielectric surface, micro-discharge, fluid model

PACS: 52.25.Mq, 52.30.–q, 52.65.–y, 52.65.Kj

DOI: 10.1088/1674-1056/ada43d **CSTR:** 32038.14.CPB.ada43d

1. Introduction

Without the need for a vacuum chamber, dielectric barrier discharge (DBD) can be easily used in batch processing, which has become a popular approach to producing atmospheric pressure non-thermal plasma.[1] Due to its various merits, DBD has extensive application potentials, such as surface modification,[2,3] flow control,[4,5] biomedical sterilization,[6,7] and pollution abatement.[8–10]

Different to traditional discharges conducted with parallel electrodes at low pressure, DBD is characterized by inserting at least one dielectric layer into the discharge gap.[11,12] After initiation, charged particles are accumulated on the dielectric surfaces, which induce a field contradictory to the applied one and then make the discharge quench. Hence, DBD can only be ignited repeatedly at different half periods of an alternating current voltage, suppressing the instability that leads to arc discharge.[13,14] Under most cases, DBD appears as some stochastically distributed filaments. Thanks to the unremitting efforts of the plasma community, experimental parameters including voltage,[15–17] frequency,[18] gas flow rate,[19] and impurity content[20,21] have been investigated for DBD.[22,23]

In fact, gap width (d_g) is a paramount parameter to determine discharge aspects and plasma characteristics,[24] which along with pressure (p) dictates the discharge regime (a Townsend regime under a low pd_g and a streamer regime under a high pd_g).[25] In addition to a uniform gap, DBD can also be performed with a non-equal gap, which can be caused, for example, by a slight inclination of one electrode.[26] With a non-equal gap, DBD does not initiate simultaneously, but first occurs at the position with the narrowest gap,[14,27] then propagates to the next position with a relatively wider gap.[26,28] Replacing traditional smooth-surface dielectric with topographic relief insulators, patterns are formed because DBD initiations are repeatedly and exclusively nucleated at the tips of the dielectric pyramids.[29] In addition, when one dielectric layer has a wavy surface,[30,31] micro-discharges tend to appear at the valleys during the positive discharge and at the crests during the negative discharge, constituting a complimentary pattern.

In this paper, DBD with both of the dielectric layers hav-

†Corresponding author. E-mail: plasmalab@126.com

© 2025 Chinese Physical Society and IOP Publishing Ltd. All rights, including for text and data mining, AI training, and similar technologies, are reserved.

ing a wavy surface is numerically simulated based on a two-dimensional fluid model. By varying the relative position (phase difference) between the two wavy surfaces, different self-organized patterns are obtained.

2. Model description

Figure 1 shows a schematic diagram of the model to simulate DBD with two wavy dielectric surfaces. Two square plate electrodes with a length of 10.0 mm are covered by dielectric layers (relative permittivity of 7.5), with a length of 12.0 mm. Considering the geometry of the discharge device, a two dimensional model is adopted and the wavy surfaces of the dielectrics are expressed as follows:

$$\text{Lower dielectric: } y = 1 - 0.1 \times \cos(\pi x), \tag{1}$$

$$\text{Upper dielectric: } y = 3 - 0.1 \times \cos(\pi x + \Delta\varphi), \tag{2}$$

where $\Delta\varphi$ is the phase difference between the two wavy surfaces. Results indicate that the number of micro-discharges increases as the period of surface profile shortens. In our work, pattern formation of filaments is intended to be investigated, which actually requires sufficient micro-discharges to make them self-organized. Hence, a relatively short period of 2.0 mm is chosen, which is the same to that used in Ref. [32]. The initial phase of the lower surface is fixed at zero, while that of the upper surface varies, leading to the change of $\Delta\varphi$. When $\Delta\varphi = 0$, the upper surface has the same waveform with the lower one. When $\Delta\varphi = \pi/2$, the waveform of the upper surface shifts to the left by 0.5 mm. Dielectric thickness fluctuates from 0.9 mm (valley) to 1.1 mm (crest), resulting in a gap width ranging from 1.8 mm to 2.2 mm. The z-direction depth of the model is 20. mm. Pressure and temperature of helium with trace nitrogen (100 ppm) are maintained at 760 Torr (1 Torr = 1.33322×10^2 Pa) and 300 K, respectively. The upper electrode is driven with a 10.0-kHz sinusoidal voltage (4.0-kV amplitude), and the lower electrode is grounded.

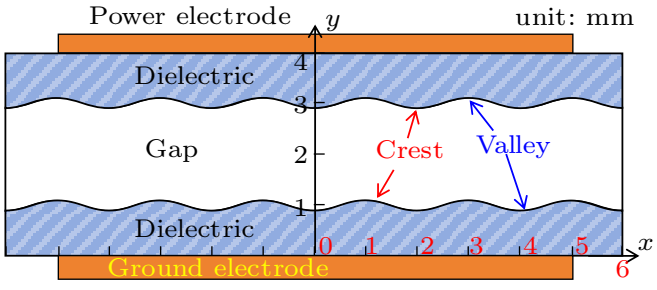


Fig. 1. Schematic diagram of the model geometry.

In this model, the governing equations of electron properties are simplified to the continuity equations based on the drift-diffusion approximation.[32,33] The transport of heavy species is determined by the multi-component diffusion equation.[34] Moreover, electric field (E) is solved by Poisson's equation. On the dielectric surfaces, the secondary electron emission coefficient by bombardment is set to 0.01 for helium ions with an initial electron energy of 5.0 eV and 0.001 for nitrogen-molecule ions with an initial electron energy of 3.0 eV.[35] In the gap, we have considered 9 particles (i.e., electron (e), He, He*, He_2^* , He^+, He_2^+, N_2, N_2^+, and N_4^+) and 27 reactions,[36] whose rate coefficients are calculated in BOLSIG+[37] using the cross-section data[38] or taken from Ref. [36]. A homogeneous initial condition is employed in the gap for all species. Considering electroneutrality, initial e, He^+, He_2^+, N_2^+, and N_4^+, are set to 2.2×10^{13} m^{-3}, 1×10^{13} m^{-3}, 1×10^{13} m^{-3}, 1×10^{12} m^{-3}, and 1×10^{12} m^{-3}, respectively. On the dielectric surfaces, 6 reactions are considered.[36]

The simulation is performed in COMSOL Multiphysics with 322672 total number of freedom degrees. The mesh consists of 48000 elements, whose minimal size in the gap is 5 μm×40 μm close to the dielectric surfaces. The minimal and average values of mesh quality are 0.7185 and 0.9210, respectively, which are similar to those reported by others.[39] The model has been verified by parallel-plate DBD with plain dielectric surfaces.[36] Usually, a steady state can be reached for a DBD with plain dielectric surface after typically 8–10 voltage cycles.[40] For a wavy dielectric surface, it takes only 4 voltage cycles to reach a steady state.[31] To ensure the discharge has reached a steady state, the results are obtained after 10 voltage cycles.

3. Results and discussion

To validate the model, waveforms of voltages and current density are presented in Fig. 2(a) for DBD with plain dielectric surface. As can be seen, there is only one discharge pulse per voltage cycle, whose peak value is about 1.76 mA/cm^2. In addition, just before the polarity change of applied voltage, gap voltage increases with time, which induces the discharge at gap voltage of about 750 V. The peak value of current density and the gap voltage for initiation are in line with those presented in Ref. [36], which verifies the validity of our model.

Figure 2(b) presents waveforms of applied voltage and discharge current density with $\Delta\varphi$ corresponding to 0, $\pi/2$, and π, respectively. For a given $\Delta\varphi$, there is a positive discharge and a negative discharge per voltage cycle, both of which consist of a pulse stage and a hump stage. According to the current continuum equation, the total current (j_t) is the sum of the conduction current (j_c) and the displacement current ($\varepsilon\partial E/\partial t$), where ε is the permittivity, taking ε for the gas gap and $\varepsilon_0\varepsilon_\mathrm{r}$ for the dielectric barriers.[41] In addition, $j_\mathrm{c} = q(\Gamma_\mathrm{i} - \Gamma_\mathrm{e})$,[42] here $q\Gamma_\mathrm{i}$ and $-q\Gamma_\mathrm{e}$ are ion current density and electron current density, respectively, which can be directly got from COMSOL. The current waveform in

Fig. 2(b) corresponds to j_c, which does not contain the displacement current. Hence, the hump stage should not come from the displacement current, but correspond to a discharge event. Moreover, the current profile is identical for the positive discharge and the negative discharge. With increasing $\Delta\varphi$, maximal current monotonously rises for the pulse stage while keeping almost constant for the hump stage. It is noteworthy that the discharge initiates prior to the polarity reversal of applied voltage, similar to DBD with plain dielectrics.[43] This phenomenon suggests that surface charge on the dielectrics plays a predominant role in the discharge.

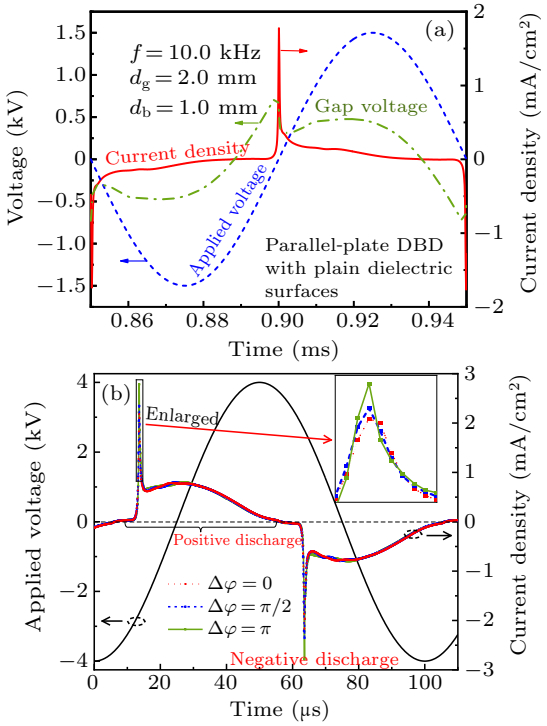


Fig. 2. Waveforms of voltage and current density for DBD with the plain-surfaces (a) and the wavy surfaces for different $\Delta\varphi$ (0, $\pi/2$, π) (b).

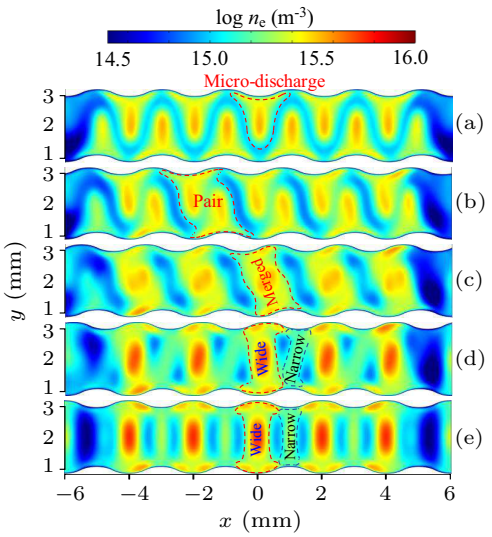


Fig. 3. Spatial distribution of ne (on a log scale) averaged in one voltage cycle with $\Delta\varphi = 0$ (a), $\pi/4$ (b), $\pi/2$ (c), $3\pi/4$ (d), and π (e).

Figure 3 indicates spatial distribution of electron density (n_e) averaged over one voltage period with different $\Delta\varphi$. Different self-organized patterns are observed for the micro-discharges (MDs) with varying $\Delta\varphi$. One can see that the MDs are arranged vertically with equal intervals when $\Delta\varphi = 0$, whose width is the largest in the vicinity of the surface crests and shrinks with increasing distance away from the crests. With increasing $\Delta\varphi$, the MDs become slightly stronger and tilted. The tilted MDs are self-organized into several pairs with equal intervals ($\Delta\varphi = \pi/4$). When $\Delta\varphi$ is elevated to $\pi/2$, the MDs in a pair are merged. The pattern with the merged MDs has a higher n_e than the MD pairs. With $\Delta\varphi = 3\pi/4$, wide bright MDs bridge the facing valleys of the upper and lower dielectrics, between which narrow dim MDs appear bridging two dielectric crests. The boundary is unclear between the wide and the narrow MDs near the wavy surfaces. When $\Delta\varphi = \pi$, the wide and the narrow MDs turn vertical, which alternately appear along the x axis.

As mentioned above, the positive discharge has a current profile identical to that of the negative discharge, meaning their similar evolution. Hence, only the positive discharge is investigated in the following (Figs. 4, 6, and 7). For the positive discharge, the upper dielectric serves as the instantaneous anode. In Figs. 4, 6, and 7, n_{em} and E_m refer to the maximal value of n_e (in units of m^{-3}) and E (in units of kV/cm), respectively. As will be shown later, the valleys have more surface charges than the crests. Hence, a great number of residual electrons left by the previous discharge are attracted at the anode valleys just before the initiation of the positive discharge (10.0 μs).

Owing to the dielectric polarization,[44,45] E is enhanced near the crests. That is to say, the first Townsend ionization (α) coefficient is higher near the crests in contrast to that near the valleys. As a result, more electrons are produced, and the discrete MDs are observed near the upper crests. Except for those at the electrode edge, the MDs almost follow a similar variation trend with time. Hence, we take the MD (centered at the dashed line in Fig. 4) as an example. After initiation (12.0 μs), electron density increases with increasing distance from the instantaneous cathode (the lower dielectric) due to impact ionization. It can be inferred that the MD operates in a Townsend-like discharge mode considering that n_{em} appears in the vicinity of the anode.[46,47] Positive ions (referred to as ions in the following) in the MD drift almost vertically downward, which are going to be accumulated above the lower valley and enhance E there (13.2 μs). Accelerated by the enhanced E, ions impact the lower dielectric surface to release secondary electrons. During their upward drift, the electrons are multiplied in the enhanced E region. Hence, n_{em} of the MD increases with time. In addition, a low-E region in the MD is formed owing to the production of high-density electrons. At 13.6 μs (the maximal current moment of the pulse stage), the region of n_{em} reaches the vicinity of the cathode. Moreover,

a cathode-fall region with E_m of about 12 kV/cm is formed near the lower dielectric, suggesting that the MD operates in the glow-like discharge mode.[47,48] Therefore, the MD in the pulse stage transits from the Townsend-like discharge mode to the glow-like discharge one, which is similar to that found in DBD with plain dielectric surfaces.[46,48]

After the pulse peak moment (13.8 μs), less electrons and ions are produced with reducing current. Accordingly, n_{em} decreases with time. With less ions to enhance E near the cathode, E_m also decreases with time. At 16.0 μs, n_{em} appears near the anode (similar to a Townsend-like discharge), while E_m appears near the cathode (similar to a glow-like discharge). Hence, the MD operates in a mixed mode. When applied voltage changes its polarity, E is enhanced again (20 μs). Even though, n_e decreases remarkably, and the MD is maintained with a relatively low n_e (24.4 μs). Then, n_{em} and E_m decrease with time (30 μs) before the MD quenches at last. Compared Fig. 3 with Fig. 4, one can assert that the only half of the MDs in Fig. 3 are generated during the positive discharge. Hence, the other half of the MDs will be generated during the negative discharge. In addition, the MDs in the positive discharge are complementary to those in the negative discharge.

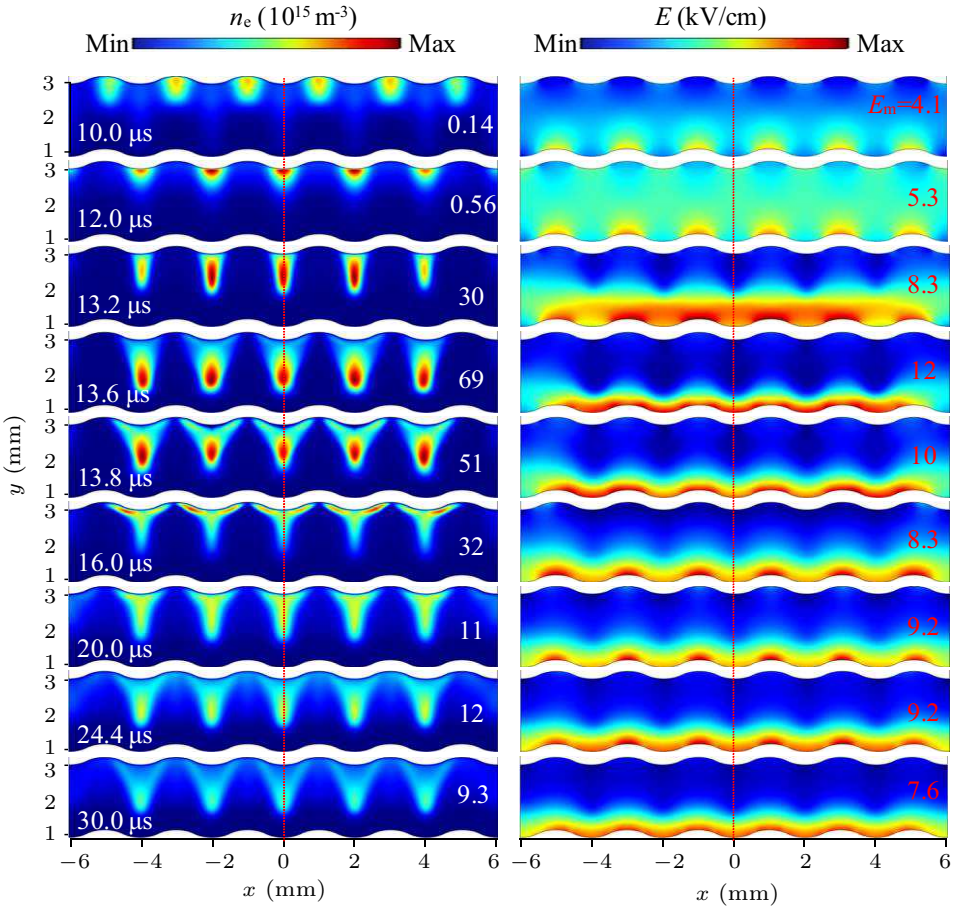


Fig. 4. Evolutions of n_e and E with $\Delta\varphi = 0$ for the positive discharge. The labeled numbers in the left column multiply 10^{15} equal n_{em}, and the numbers in the right column correspond to E_m.

The discharge seems to return to the anode side from 13.8 μs to 16.0 μs, which can be discussed as follows. Figure 5 indicates spatial distribution of total ionization rate (R_e) at 13.6 μs, 13.8 μs, and 16.0 μs with $\Delta\varphi = 0$ (corresponding to Fig. 4). In addition, the orientation and size of the arrows correspond to the direction and magnitude of electron flux (Γ_e), respectively. It can be seen from Fig. 5 that from 13.6 μs to 16.0 μs, maximal R_e always appears at the vicinity of the instantaneous cathode due to the existence of the cathode fall region. This means that electrons are mainly produced at the vicinity of the cathode (the lower dielectric). The electrons born near the lower dielectric will drift upward (see the arrows). After they reach the vicinity of the upper dielectric, electrons are gradually trapped by the valleys of the upper dielectric due to the horizontal component of the electric field. Therefore, n_{em} appears near the anode at 16.0 μs. Hence, in the mixed mode, electrons are mainly produced in the cathode fall region near the lower dielectric although n_{em} appears in the vicinity of the anode near the upper dielectric.

In addition, the average electron energy of DBD is several eV,[49] which corresponds to a reaction rate coefficient (k) from 10^{-18} m^3/s to 10^{-17} m^3/s calculated by BOLSIG+. In the discharge, n_e is 10^{16} m^{-3}, and helium atom density (N) is approximately 10^{25} m^{-3} at atmospheric pressure. As a result,

$R_e = k \times n_e \times N = 10^{23}$ m^{-3}·s^{-1}–10^{24} m^{-3}·s^{-1}, as presented in Fig. 5, which is actually on one order of magnitude higher than the axis-averaged R_e (result not shown here). Hence, the axis-averaged R_e is on one order of magnitude lower than that reported in Ref. [36]. The lower R_e is attributed to the lower n_e of DBD with the wavy dielectric surfaces.

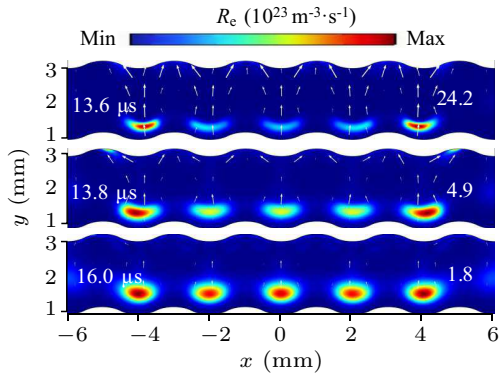


Fig. 5. Spatial distribution of R_e at 13.6 μs, 13.8 μs, and 16.0 μs with $\Delta\varphi = 0$. The orientation and size of the arrows correspond to the direction and magnitude of Γ_e, respectively. The labeled numbers multiply 10^{23} correspond to maximal R_e.

Figure 6 depicts temporal evolutions of n_e and E for the positive discharge with $\Delta\varphi = \pi/2$, which in general are similar to those with $\Delta\varphi = 0$. The difference lies in the fact that the MD is vertical with $\Delta\varphi = 0$, while tilted or even deviated from the dashed line with $\Delta\varphi = \pi/2$. From 12.0 μs to 13.6 μs, a large number of ions drift towards the lower dielectric (almost along the dashed line). When they reach the vicinity of the instantaneous cathode, E is stronger on the left side of the dashed line compared with that on the right side due to the polarization of the lower dielectric. Hence, ions are attracted to enhance E further on the left side (13.6 μs), producing more electrons on the left side of the MD, as can be seen in Fig. 6. Moreover, a horizontal field component is induced by the spatial ions accumulated above the lower dielectric, which directs the ions to move to the right side (In fact, also to the left side, however, for the movement to the left the spatial ions encounters the rising edge of the dielectric crest, reducing surface charges and weakening E on the left side). Hence, E on the right side is enhanced and that on the left side is weakened (13.8 μs). With the strengthening E, the multiplication process of electrons (the production of equal amounts of ions) is improved on the right side. One can see that n_{em} near the upper crest is higher on the right side (16.0 μs). As a result, more ions drift downward to enhance E on the right side. Apparently, this is a positive feedback process, which enhances the discharge on the right and weakens that on the left. Consequently, the MD moves to the right side of the dashed line (from 20.0 μs to 30.0 μs).

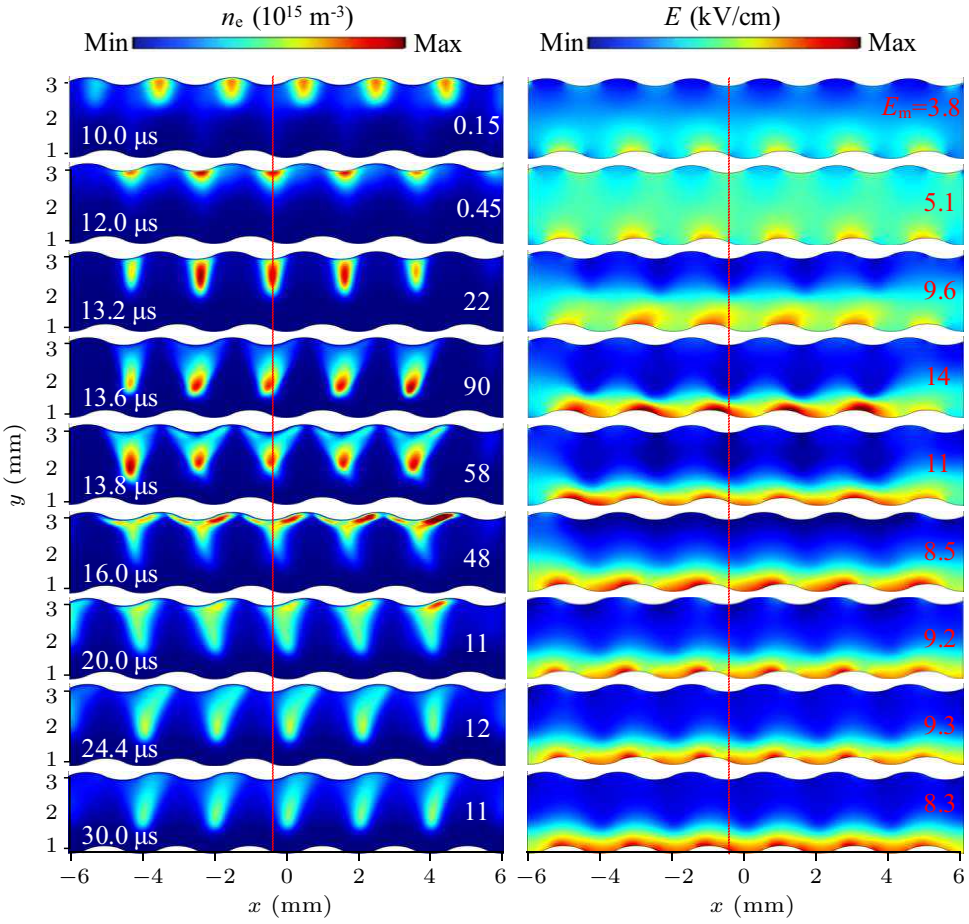


Fig. 6. Evolutions of n_e and E with $\Delta\varphi = \pi/2$ for the positive discharge. The labeled numbers in the left column multiply 10^{15} equal n_{em}, and the numbers in the right column correspond to E_m.

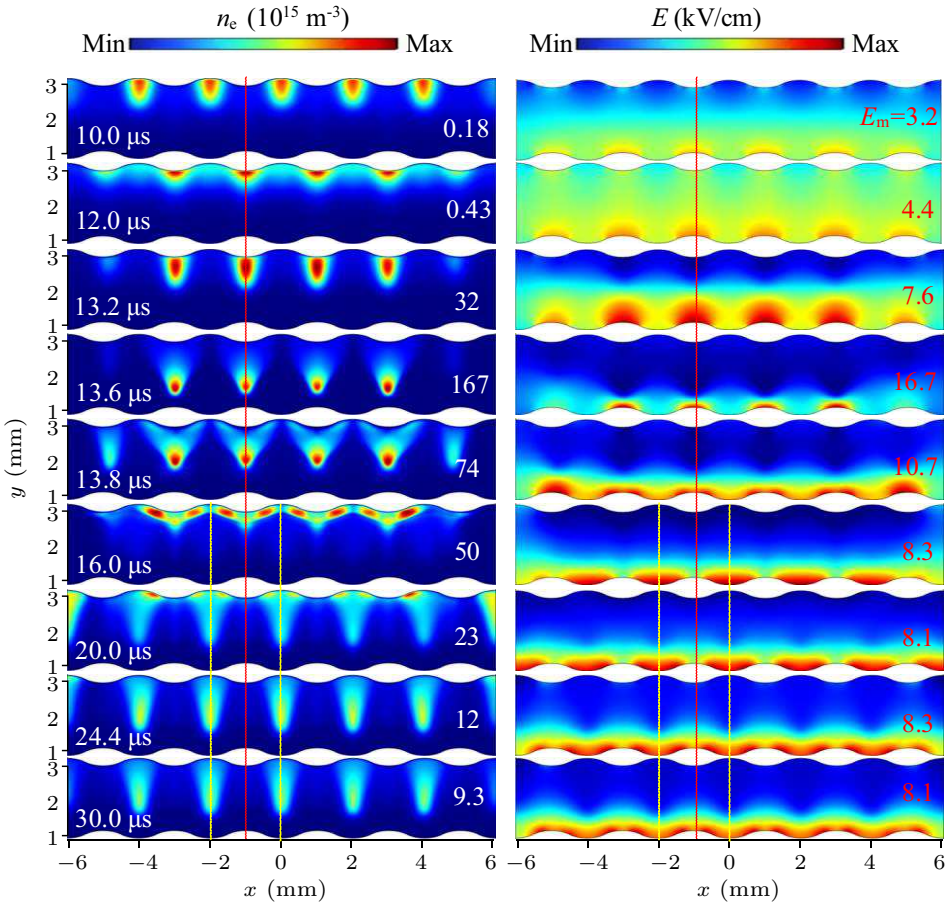


Fig. 7. Evolutions of n_e and E with $\Delta\varphi = \pi$ for the positive discharge. The labeled numbers in the left column multiply 10^{15} equal n_{em}, and the numbers in the right column correspond to E_m.

Figure 7 illustrates temporal evolutions of n_e and E for the positive discharge with $\Delta\varphi = \pi$. In the pulse stage (from 12.0 μs to 13.6 μs), the evolutions are similar to those of $\Delta\varphi = 0$ or $\pi/2$. However, spatial ions are accumulated near the lower crest with $\Delta\varphi = \pi$. At 13.8 μs, spatial ions move to the two neighboring valleys under the effect of the horizontal field component. The redistribution of ions above the lower dielectric result in E decrement near the crest and relative E increment near the valleys. Consequently, more electrons are produced above the lower valleys, and n_e decreases near the red dashed line (16.0 μs). Due to the positive feedback process, the discharge weakens near the red line, while strengthens near the yellow lines. At last, the MD centered at the red line bridging the upper and lower crests shifts to the MD centered at the yellow line bridging the upper and lower valleys (20.0 μs to 30.0 μs). It is worth noting that n_{em} of the MD is 1.67×10^{17} m^{-3} at 13.6 μs, while 2.3×10^{16} m^{-3} at 24.4 μs. The MD with the higher n_{em} in Fig. 7 corresponds to the narrow dim MD in Fig. 3, while that with the lower n_{em} corresponds to the wide bright one in Fig. 3. The reason can be discussed as follows. Figure 3 is a time-averaged spatial distribution, that is, its brightness is related to not only n_{em}, but also the discharge duration. The narrow dim MD has a discharge duration much shorter than the wide bright MD.

From Figs. 4, 6, and 7, one can see that n_{em} is on the order of magnitude of 10^{16} m^{-3}, which is slightly lower than that in atmospheric pressure plasma. As to the low electron density, we can explain as follows. In parallel-plate DBD with plain dielectric surface, n_{em} has been reported on the order of magnitude of 10^{16} m^{-3} in some Refs. [50–52], which can reach a high value of 10^{17} m^{-3}–10^{18} m^{-3}. The lower n_{em} can be attributed to the relief topography of the instantaneous electrode (the dielectric). Due to the relief topography, the reduced field is remarkably decreased than those in DBD with plain dielectric surface (about 100 Td). Therefore, DBD with relief surfaces has a lower electron temperature.[49] The decrement in reduced field and electron temperature lead to decrement in α coefficient, which further results in the decrement in electron density. For DBD with wavy dielectric surfaces, the reduced field at 13.6 μs (the moment of current peak) is roughly 51.8 Td ($\Delta\varphi = 0$), which is only half of that in DBD with plain surface. Therefore, n_{em} of the discharge with wavy surfaces is lower than DBD with plain dielectric surface.

Figure 8 shows surface charge density on the upper (left) and lower (right) dielectrics for the positive discharge with $\Delta\varphi = 0$, $\pi/2$, and π, in which the black dotted lines label the valley bottoms. It is obvious that surface charge is non-uniformly distributed for a given moment, and the valleys pos-

sess more surface charge than the crests. Due to the non-uniform distribution of surface charge (10.0 μs), more residual electrons are attracted near the upper valleys just before the positive discharge (Figs. 4–6). As the positive discharge sustains from 10.0 μs to 35.0 μs, surface charge of the upper dielectric gradually reduces in quantity, which keeps positive until electrons are deposited on the surface. Accordingly, the lower dielectric undergoes an opposite process. In addition, the distributions of surface charge with $\Delta\varphi = 0$ and π are symmetric about the valleys (or the crests). However, it is asymmetric with $\Delta\varphi = \pi/2$, especially at 24.4 μs and 35.0 μs, which corresponds to the asymmetric evolution of the MDs. Interestingly, after the discharge extinguishment from 35.0 μs to 56.0 μs, surface charge continues increasing. This phenomenon can be attributed to lots of residual ions and electrons in the discharge region, which continue drifting to increase surface charge on the dielectrics.

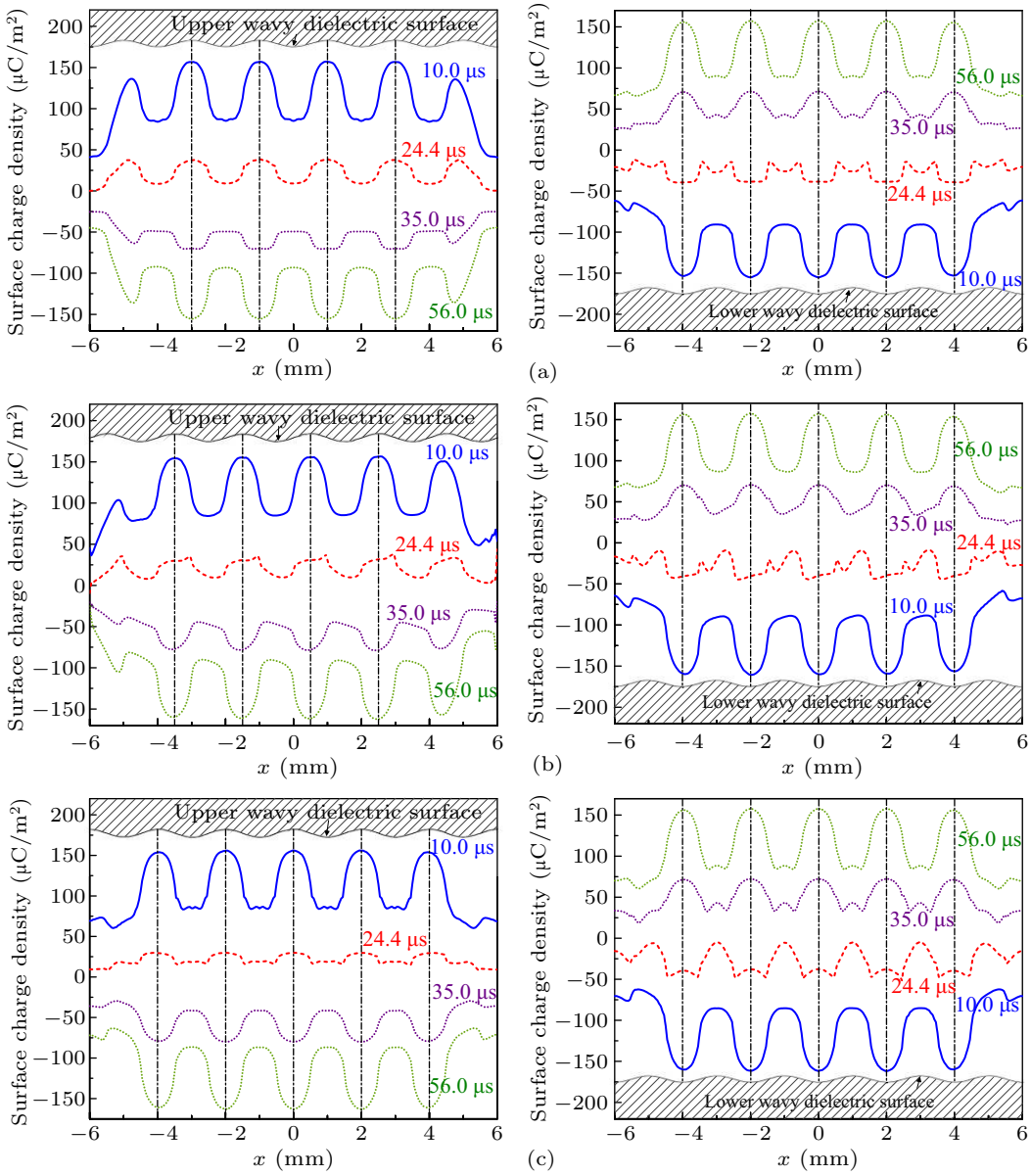


Fig. 8. Distribution of surface charge on the upper dielectric (left) and the lower dielectric (right) for different moments of the positive discharge: $\Delta\varphi = 0$ (a), $\pi/2$ (b), and π (c).

4. Conclusion

In summary, atmospheric pressure DBD with two wavy dielectric surfaces has been numerically simulated in helium mixed with trace nitrogen based on a two-dimensional fluid model. The simulation results indicate that there is a positive discharge and a negative discharge per voltage cycle, both of which are composed of the pulse stage and the hump stage. The maximal current of the pulse stage increases, while that of the hump stage keeps almost constant with increasing $\Delta\varphi$. In addition, DBD with wavy dielectric surfaces appears as the discrete MDs, which are self-organized in different patterns with varying $\Delta\varphi$. With $\Delta\varphi = 0$, the equal-internal MDs

are vertical, which become tilted and appear as pairs with $\Delta\varphi = \pi/4$. The MD pairs are merged into bright wide MDs with $\Delta\varphi = \pi/2$. With $\Delta\varphi = 3\pi/4$, the self-organized pattern is composed of the wide and narrow MDs, which appear alternately. The tilted MDs turn vertical with $\Delta\varphi = \pi$. The evolutions of n_e and E reveal that there is a transition from the Townsend-like discharge mode to the glow-like discharge mode in the pulse stage. Moreover, a mixed discharge mode is formed in the hump stage. With $\Delta\varphi = 0$, the MDs are always centered at the lines connecting the upper crests and the corresponding lower valleys. They shift at the hump stage to the right side of the original positions of the MDs with $\Delta\varphi = \pi/2$. With $\Delta\varphi = \pi$, the MDs centered at the lines connecting the upper and lower crests evolve into those centered at the lines bridging the upper and lower valleys. In addition, surface charge on the upper and lower dielectrics has been analyzed at last.

Acknowledgements

Project supported by the National Natural Science Foundation of China (Grant Nos. 12375250, 11875121, 51977057, and 11805013), the Natural Science Foundation of Hebei Province, China (Grant Nos. A2020201025 and A2022201036), the Hebei Province Optoelectronic Information Materials Laboratory Performance Subsidy Fund Project (Grant No. 22567634H), the Funds for Distinguished Young Scientists of Hebei Province, China (Grant No. A2012201045), the Natural Science Interdisciplinary Research Program of Hebei University (Grant Nos. DXK201908 and DXK202011), and the Post-graduate's Innovation Fund Project of Hebei University (Grant No. HBU2022bs004).

References

[1] Brandenburg R 2017 *Plasma Sources Sci. Technol.* **26** 053001
[2] Rincón R, Hendaoui A, Matos J and Chaker M 2016 *J. Appl. Phys.* **119** 223303
[3] Shao T, Yang W J, Zhang C, Niu Z, Yan P and Schamiloglu E 2014 *Appl. Phys. Lett.* **105** 071607
[4] Zheng J G 2021 *Chin. Phys. B* **30** 034702
[5] Yang H S, Zhao G Y, Liang H and Wei B 2020 *Chin. Phys. B* **29** 105203
[6] Guo Y T, Fang M Q, Zhang L Y, Sun J J, Wang X X, Tie J F, Zhou Q, Zhang L Q and Luo H Y 2022 *Appl. Phys. Lett.* **121** 074101
[7] Babaeva N Y, Tian W and Kushner M J 2014 *J. Appl. Phys.* **47** 235201
[8] Mei D H, Zhu X B, He Y L, Yan J D and Tu X 2015 *Plasma Sources Sci. Technol.* **24** 015011
[9] Rathore V, Pandey A, Patel S, Dave H and Nema S 2024 *Phys. Scr.* **99** 035602
[10] Li S J, Dang X Q, Yu X, Abbas G, Zhang Q and Cao L 2020 *Chem. Eng. J.* **388** 124275
[11] Li X C, Chu J D, Zhang Q, Zhang P P, Jia P Y and Geng J L 2016 *Appl. Phys. Lett.* **109** 204102
[12] Wu K Y, Wu J C, Jia B Y, Ren C H, Kang P C, Jia P Y and Li X C 2020 *Phys. Plasmas* **27** 082308
[13] Shi J J, Liu D W and Kong M G 2006 *Appl. Phys. Lett.* **89** 081502
[14] Liu J, Yang Y, Nie L, Liu D and Lu X 2024 *J. Phys. D: Appl. Phys.* **57** 275201
[15] Pipa A V, Hink R, Foest R and Brandenburg R 2020 *Plasma Sources Sci. Technol.* **29** 12LT01
[16] Zhang D X, Yu J X, Li M Y, Pan J, Liu F and Fang Z 2023 *Plasma Sci. Technol.* **25** 114004
[17] Zhang J, Cheng W, Wang Y H and Wang D Z 2022 *Phys. Plasmas* **29** 103505
[18] Gou X X, Yuan D K, Wang L J, Xie L J, Wei L S and Zhang G X 2023 *Vacuum* **212** 112047
[19] Tang M, Tang J F, Zhou D S and Yu D R 2021 *Phys. Plasmas* **28** 050701
[20] Hong Y, Ning W J, Dai D and Zhang Y H 2020 *Phys. Plasmas* **27** 053510
[21] Zhang Y H, Ning W J, Dai D and Wang Q 2019 *Plasma Sources Sci. Technol.* **28** 075003
[22] Liu G M, Chen L, Zhao Z B and Song P 2023 *Chin. Phys. B* **32** 125205
[23] Bazinette R, Sadeghi N and Massines F 2020 *Plasma Sources Sci. Technol.* **29** 095010
[24] Dai D, Hou H X and Hao Y B 2011 *Appl. Phys. Lett.* **98** 131503
[25] Wu S, Wang Z, Huang Q J, Wang W, Yu S, Zou C L, Lu Y and Lu X P 2014 *IEEE Trans. Plasma Sci.* **42** 2342
[26] Li Z Y, Jin S H, Xian Y B, Nie L L, Liu D W and Lu X P 2021 *Plasma Sources Sci. Technol.* **30** 065026
[27] Jin S H, Zhao F, Nie L L, Liu D W and Lu X P 2022 *Plasma Process. Polym.* **19** 2200021
[28] Jin S H, Li Z Y, Xian Y B, Nie L L and Lu X P 2022 *High Voltage* **7** 98
[29] Polonskyi O, Hartig T, Uzarski J R and Gordon M J 2021 *Appl. Phys. Lett.* **119** 211601
[30] Wang Q, Ning W J, Dai D and Zhang Y H 2019 *Plasma Process. Polym.* **17** 1900182
[31] Liu K, Fang Z and Dai D 2023 *Acta Phys. Sin.* **72** 135201 (in Chinese)
[32] Ren C H, He X R, Jia P Y, Wu K Y and Li X C 2020 *Phys. Plasmas* **27** 113507
[33] Jia P Y, Ran J X, Wu J C, Wang D D, Wu K Y, He X R and Li X C 2022 *J. Phys. D: Appl. Phys.* **56** 015203
[34] Jia P Y, Wan W J, Zhang L L, Ran J X, Wu K Y, Wu J C, Pang X X and Li X C 2023 *AIP Adv.* **13** 065005
[35] Lazarou C, Belmonte T, Chiper A S and Georghiou G E 2016 *Plasma Sources Sci. Technol.* **25** 055023
[36] Wang Q, Ning W J, Dai D, Zhang Y H and Ouyang J T 2019 *J. Phys. D: Appl. Phys.* **52** 205201
[37] Hagelaar G J M and Pitchford L C 2005 *Plasma Sources Sci. Technol.* **14** 722
[38] IST-Lisbon database (https://lxcat.net/)
[39] Li X C, Wang D D, Chen J Y, Wu J C, Zhao N, Jia P Y and Wu K Y 2022 *Phys. Fluids* **34** 027112
[40] Zhang P and Kortshagen U 2006 *J. Phys. D: Appl. Phys.* **39** 153
[41] Gao S H, Wang X C and Zhang Y T 2020 *Acta Phys. Sin.* **69** 115204 (in Chinese)
[42] Wang J, Lei B Y, Li J, Xu Y G, Zhang J Y, Tang J, Wang Y S, Zhao W and Duan Y X 2019 *Phys. Plasmas* **26** 013511
[43] Liu F C, Wang X F, He Y F and Dong L F 2016 *Phys. Plasmas* **23** 032301
[44] Li X C, Zhang L L, Chen K, Ran J X, Pang X X and Jia P Y 2024 *IEEE Trans. Plasma Sci.* **52** 1619
[45] Jahanbakhsh S, Brüeser V and Brandenburg R 2018 *Plasma Sources Sci. Technol.* **27** 115011
[46] Luo H Y, Liang Z, Lv B, Wang X X, Guan Z C and Wang L M 2007 *Appl. Phy. Lett.* **91** 221504
[47] Luo H Y, Liang Z, Wang X X, Guan Z C and Wang L N 2010 *J. Phys. D: Appl. Phys.* **43** 155201
[48] Chen M, Dong X Q, Wu K Y, Ran J X, Jia P Y, Wu J C and Li X C 2024 *Appl. Phy. Lett.* **124** 214102
[49] Sun Y Z, Dong K L, Xu Z L and Zhang Y 2018 *Res. Phys.* **11** 999
[50] Lu B, Wang X X, Luo H Y and Liang Z 2009 *Chin. Phys. B* **18** 646
[51] Li X C, Niu D Y, Xu L F, Jia P Y and Chang Y Y 2012 *Chin. Phys. B* **21** 075204
[52] Huang Z M, Hao Y P, Yang L, Han Y X and Li L C 2015 *Phys. Plasmas* **22** 123509